

Rotating systems, universal features in dragging and anti-dragging effects, and bounds onto angular momentum

Janusz Karkowski, Patryk Mach,^{*} Edward Malec,[†] and Michał Piróg
Instytut Fizyki im. Mariana Smoluchowskiego, Uniwersytet Jagielloński, Łojasiewicza 11, 30-348 Kraków, Poland

Naqing Xie[‡]
School of Mathematical Sciences, Fudan University, Shanghai, China

We consider stationary, axially symmetric toroids rotating around spinless black holes, assuming the general-relativistic Keplerian rotation law, in the first post-Newtonian approximation. Numerical investigation shows that the angular momentum accumulates almost exclusively within toroids. It appears that various types of dragging (anti-dragging) effects are positively correlated with the ratio M_D/m (M_D is the mass of a toroid and m is the mass of the black hole) — moreover, their maxima are proportional to M_D/m . The horizontal sizes of investigated toroids range from c. 50 to c. 450 of Schwarzschild radii R_S of the central black hole; their mass $M_D \in (10^{-4}m, 40m)$ and the radial size of the system is c. 500 R_S . We found that the relative strength of various dragging (anti-dragging) effects does not change with the mass ratio, but it depends on the size of toroids.

Several isoperimetric inequalities involving angular momentum are shown to hold true.

I. INTRODUCTION

There are three principal aims of this paper.

We have found recently two new weak field effects that affect angular velocities of gaseous disks rotating around spinless black holes [1, 2]. They appear in the first post-Newtonian approximation (1PN hereafter), in addition to the well known geometric dragging of frames. One of them — we call it anti-dragging, since it works against the dragging of frames — is proportional to the speed of sound of gas. The other depends on a combination of gravitational and centrifugal potentials, that strictly vanishes for weightless disks. All 1PN corrections strictly vanish for uniformly rotating disks, but they are nonzero for the important case of the Keplerian rotation.

We shall address in this paper the following question: what are the principal physical properties of a (Keplerian) rotating toroidal-black-hole system, that are responsible for the strength of various dragging (anti-dragging) effects? One can expect — by appealing to the behaviour of test particles in the Kerr geometry — that robust dragging phenomena should be associated with compact systems that possess a lot of angular momentum. Our investigation shows that this intuition is incorrect, and that the relevant characteristic is the mass ratio M_D/m , where M_D is the mass of a toroid and m is the mass of the black hole. We find an interesting universality: the maxima of the combined, normalized in a suitable sense, (1PN) corrections, as well of its constituents — the geometric dragging, the anti-dragging, and the centrifugal one [2] — are simply proportional to M_D/m , for a fixed extension of a toroid. We have studied polytropic disks for two classes of polytropes; the universality

appears in all examples, but some numerical coefficients depend (albeit rather weakly) on the equation of state of the fluid.

An interesting question is the influence of a rotating environment onto the central black hole. There are reports — for a rigid rotation [3, 4] and the constant specific angular momentum [5] — that the black hole can carry substantial amount of the angular momentum. We assume a general-relativistic version of the Keplerian rotation law [2]. It comes as a surprise, that one can have compact systems with a large amount of angular momentum, where central black holes practically do not participate in rotation — their spin parameters are smaller than 10^{-4} , and they carry less than one-millionth of the total angular momentum.

Finally, there exist several inequalities that must be obeyed by quasilocal characteristics of apparent horizons. S. Dain extended these by formulating local estimates onto local angular momentum of rotating bodies, and proved them, under somewhat stringent conditions [6, 7]. We show that they are in fact satisfied.

The order of the rest of this paper is as follows. In the next section we formulate axial perturbations of the conformal Schwarzschild geometry, that describe toroids rotating around a spinless black hole. The basic idea is to build systems such that the gravity of toroids is negligible — compared to the gravity of the central black hole — close to the event horizon, and the gravitational potential is small within the bulk of rotating matter. The rotation is ruled by the general-relativistic Keplerian law. Section III shows the first post-Newtonian approximation to equations of motion. Section IV is dedicated to the quasilocal description of the system, in particular to defining the concept of the apparent horizon, its mass and its angular momentum. We briefly describe the essence of the numerical method in Sec. V. Section VI brings main numerical results concerning various 1PN corrections to the angular velocity; we emphasise again the unexpected

^{*} patryk.mach@uj.edu.pl

[†] malec@th.if.uj.edu.pl

[‡] nqxie@fudan.edu.cn

universality of these effects. Section VII addresses the issue of distribution of the angular momentum. It appears that the black hole spin parameter $a_S \equiv c j_S / m^2$ is very small; the central black hole is almost Schwarzschildian. Only a tiny fraction of the total angular momentum can be attributed to the black hole; this is commented and explained therein. In Sec. VIII we review Dain's results on estimations of the angular momentum. Tables I and II allow one to find out that the angular momentum can be bounded, as postulated in [6]. The last section summarizes obtained results.

We assume throughout the paper the gravitational constant $G = 1$. There is a scaling freedom that allows us to treat the speed of light c as a free parameter. We adjust the speed of light c and the coordinate extension of the disk, in Secs. VI–VIII, so that the whole system has an (approximate) areal size of $500R_S$, and the inner edges of the investigated disks are located between $50R_S - 475R_S$ (again approximately). The total asymptotic mass $M_D + m$ ranges between m and $40m$. We take care to construct numerical solutions that are in the 1PN regime within the stationary toroids.

II. AXIAL PERTURBATIONS OF THE CONFORMAL SCHWARZSCHILD GEOMETRY

Einstein equations, with the signature of the metric $(-, +, +, +)$, read

$$R_{\mu\nu} - g_{\mu\nu} \frac{R}{2} = \frac{8\pi}{c^4} T_{\mu\nu}, \quad (1)$$

where $T_{\mu\nu}$ is the stress-momentum tensor. The metric is given by

$$ds^2 = -e^{\frac{2\nu}{c^2}} (dx^0)^2 + r^2 e^{\frac{2\beta}{c^2}} \left(d\phi - \frac{A_\phi}{r^2 c^3} dx^0 \right)^2 + e^{\frac{2\alpha}{c^2}} (dr^2 + dz^2). \quad (2)$$

Here $x^0 = ct$ is the rescaled time coordinate, and r, ϕ, z are cylindrical coordinates. We assume axial and equatorial symmetry, and stationarity — thus metric functions ν, α, β and A_ϕ depend only on r and z — and employ the stress-momentum tensor of the perfect fluid

$$T^{\alpha\beta} = \rho(c^2 + h)u^\alpha u^\beta + pg^{\alpha\beta}, \quad (3)$$

where ρ is the baryonic rest-mass density, h is the specific enthalpy, and p is the pressure. The Greek indices range from 0 to 3, and the Latin indices change from 1 to 3. The 4-velocity $u^\alpha = \frac{dx^\alpha}{cd\tau}$ along the world line of fluid particles (here τ is their proper time) is normalized: $g_{\alpha\beta} u^\alpha u^\beta = -1$. We introduce $u^t \equiv u^0/c$. The coordinate (angular) velocity of the fluid reads $\vec{v} = \Omega \partial_\phi$, where $\Omega = u^\phi / u^t$.

We assume the polytropic equation of state $p(\rho, s) = K(s)\rho^\gamma$, where s is the specific entropy of fluid and γ is

a constant. Then one has $h(\rho, s) = K(s) \frac{\gamma}{\gamma-1} \rho^{\gamma-1}$. The entropy is assumed to be constant.

We shall study small *stationary*, cylindrically symmetric, perturbations of the Schwarzschild spacetime, with the angular momentum being carried by a rotating disk of fluid. We consider the following geometry in the conformal (cylindrical) coordinates,

$$ds^2 = -(dx^0)^2 \left(\frac{f_+}{f_-} \right)^2 + (f_-)^4 (dr^2 + dz^2 + r^2 d\phi^2) - 2 \frac{A_\phi}{c^3} (r, z) d\phi dx^0, \quad (4)$$

where the two functions f_+ and f_- are defined as

$$f_+ = 1 + \frac{U}{2c^2}, \\ f_- = 1 - \frac{U}{2c^2}. \quad (5)$$

Here the gravitational potential U is a superposition of the central term $(-\frac{m}{R})$ and U_D , induced by the disk:

$$U = -\frac{m}{R} + U_D. \quad (6)$$

Henceforth $R = \sqrt{r^2 + z^2}$.

Let us point out that in the metric (4) the lapse function $N \equiv \frac{f_+}{f_-}$ and the shift vector $X_i = (0, 0, -A_\phi/c^3)$ are ϕ -independent.

We shall say that perturbations are small, if $|U_D|/c^2 \ll 1$. In addition, we require that within the volume V of a rotating disk $m/(Rc^2) \ll 1$; the two facts imply $|U|/c^2 \ll 1$ inside a disk. Then it is legitimate to perform the approximation procedure — the expansion in powers of $1/c^2$. It appears that the line element (4) leads to stationary equations that coincide, in the 1PN approximation, with stationary equations corresponding to the 1PN approximation of the metric (2). *Thus the two approaches are equivalent up to the 1PN order.*

The case, when the disk's potential U_D and the metric function A_ϕ do vanish, yields strictly the Schwarzschild line element. In this case the parameter m is just the asymptotic mass, the event and apparent horizons coincide and they are located at $R_h = m/(2c^2)$. We should point that the metric (4) is more convenient than (2), because it is easier to describe horizons of black holes in the class of conformal deformations of the Schwarzschild metric, than in the general metric (2). This description can be regarded as a version of the effective field approximation. Another application of the conformal factorization of the metric can be found in [8], where post-Newtonian equilibria of co-rotating neutron star binaries are investigated.

It is well known that equations of the stationary Einstein hydrodynamics are not closed; this is similar to the stationary Newtonian hydrodynamics. One needs to impose an additional closure assumption — a general-relativistic version of the “rotation curve” known in the Newtonian hydrodynamics — in order to complete the

system. In the Newtonian case one defines directly the rotation curve — the angular velocity Ω — as a prescribed function of the distance from the rotation axis. If the z -axis is the symmetry axis, then $\Omega = \Omega(r)$.

Rotation curves — angular velocities as functions of coordinates — emerge in the context of general relativity as solutions of the following three-step procedure. We define $\omega \equiv r^{-2}A_\phi$. First, notice that

$$j \equiv c^2 u_\phi u^t = \frac{v^2}{\left(\Omega - \frac{\omega}{c^2}\right) \left(1 - \frac{v^2}{c^2}\right)}, \quad (7)$$

where

$$v^2 \equiv r^2 \left(\Omega - \frac{\omega}{c^2}\right)^2 e^{-4U/c^2}, \quad (8)$$

can be interpreted as the angular momentum per unit inertial mass [9]. The resulting system is integrable if j depends only on the angular velocity Ω , $j \equiv j(\Omega)$ [10–13]. In the second step one needs to specify $j(\Omega)$, in order to close the description of a stationary system. There are few options in the existing literature, from the simple linear function $j(\Omega) = A(\Omega - B)$, where A and B are constants [10, 13], to recent nonlinear proposals of [2, 14, 15]. We adopt, following [2], the rotation law

$$j(\Omega) \equiv \frac{w^{\frac{4}{3}} \Omega^{-\frac{1}{3}}}{1 + \frac{3}{c^2} w^{\frac{4}{3}} \Omega^{\frac{2}{3}} + \frac{4\Psi}{c^2}}. \quad (9)$$

Here w and Ψ are parameters that shall be determined at each step of the post-Newtonian expansion. This choice yields the Keplerian rotation law in the Newtonian limit [2]; therefore we sometimes refer to (9) as the “general-relativistic Keplerian rotation law”.

The rotation curves $\Omega(r, z)$ can now be recovered — in the final step — from the equation

$$\frac{w^{\frac{4}{3}} \Omega^{-\frac{1}{3}}}{1 + \frac{3}{c^2} w^{\frac{4}{3}} \Omega^{\frac{2}{3}} + \frac{4\Psi}{c^2}} = \frac{v^2}{\left(\Omega - \frac{\omega}{c^2}\right) \left(1 - \frac{v^2}{c^2}\right)}. \quad (10)$$

We would like to note that the rotation law (9) leads to a new prediction, that was absent in [1], namely to the centrifugal correction $-\frac{3}{2c^2}\Omega_0\left(-\frac{m}{r} + U_{0D} + \Omega_0^2 \tilde{r}^2\right)$ to the angular velocity — see Eq. (23) in the next section, and explanations therein. It is interesting also that the weightless disk of dust rotating according to (10) satisfies exactly the Einstein equations within the Schwarzschild spacetime [2].

III. 1PN EQUATIONS WITHIN A ROTATING DISK

The 1PN equations for rotating fluids have been derived in [1] and [2], on the basis of an earlier work [16]. In this section we present a brief description of the reasoning.

The metric becomes, assuming $|U| \ll c^2$,

$$ds^2 = - \left(1 + \frac{2U}{c^2} + \frac{2U^2}{c^4}\right) (dx^0)^2 - 2c^{-3} A_\phi dx^0 d\phi + \left(1 - \frac{2U}{c^2}\right) (dr^2 + dz^2 + r^2 d\phi^2); \quad (11)$$

its spatial part is conformally flat.

The 1PN approximation can be valid if $|U| \ll c^2$.

We split different quantities (ρ , p , h , U and v^i) into their Newtonian (denoted by subscript 0) and 1PN (denoted by subscript 1) parts. This splitting reads, for the specific enthalpy h , the density ρ , the angular velocity Ω , the quantity Ψ and the potential U :

$$h = h_0 + c^{-2} h_1, \quad (12a)$$

$$\rho = \rho_0 + c^{-2} \rho_1, \quad (12b)$$

$$\Omega = \Omega_0 + c^{-2} v_1^\phi, \quad (12c)$$

$$\Psi = \Psi_0 + c^{-2} \Psi_1, \quad (12d)$$

$$U = -\frac{m}{R} + U_{0D} + c^{-2} U_1. \quad (12e)$$

The angular velocity becomes Keplerian,

$$\Omega_0 = \frac{w}{r^{3/2}}, \quad (13)$$

in the Newtonian limit. Let $M_{0D} = \int_V dV \rho_0$, where dV is the geometric volume element, denote the Newtonian mass of the disk. It appears from numerical analysis that the parameter w is close to \sqrt{m} , if $M_{0D} \ll m$. We expect (basing on numerics and partial analytical results) that in general $\sqrt{m} \leq w \leq \sqrt{m + M_{0D}}$ [17].

Notice that, up to the 1PN order,

$$\frac{1}{\rho} \partial_i p = \partial_i h_0 + c^{-2} \partial_i h_1 + \mathcal{O}(c^{-4}), \quad (14)$$

where the 1PN correction h_1 to the specific enthalpy can be written as $h_1 = \frac{dh_0}{d\rho_0} \rho_1$. For the polytropic equation of state this gives $h_1 = (\gamma - 1) h_0 \rho_1 / \rho_0$.

One can obtain the Bernoulli equations at the 0PN and 1PN orders, using the foregoing splitting into Newtonian (0PN) and 1PN parts.

The 0PN Bernoulli equation reads

$$h_0 - \frac{m}{R} + U_{0D} + \Omega_0^2 r^2 = \Psi_0, \quad (15)$$

where Ψ_0 is a constant that can be interpreted as the binding energy per unit mass. At the Newtonian level this is supplemented by the Poisson equation for the gravitational potential

$$\Delta U_{0D} = 4\pi \rho_0, \quad (16)$$

where Δ denotes the flat Laplacian.

The component A_ϕ of the shift vector satisfies the following equation

$$\Delta A_\phi - 2 \frac{\partial_r A_\phi}{r} = -16\pi r^2 \rho_0 \Omega_0. \quad (17)$$

The 1PN correction U_1 to the potential is obtained by solving the equation

$$\Delta U_1 = 4\pi [\rho_1 + 2p_0 + \rho_0(h_0 - 2U_0 + 2r^2\Omega_0^2)]. \quad (18)$$

The mass of a disk, including the 1PN correction, is given by the volume integral

$$M_D = \int_V dV \frac{1}{c^2} [\rho_1 + 2p_0 + \rho_0(h_0 - 2U_0 + 2r^2\Omega_0^2)] + M_{0D}. \quad (19)$$

Finally, we have the Bernoulli equation of the 1PN order,

$$\Psi_1 = -h_1 - U_1 - \Omega_0 A_\phi + 2r^2\Omega_0^2 h_0 - \frac{3}{2}h_0^2 - 4h_0 U_0 - 2U_0^2 - 4r^4\Omega_0^4, \quad (20)$$

where Ψ_1 is a constant.

In vacuum we are left with a pair of homogeneous elliptic equations

$$\begin{aligned} \Delta U &= 0, \\ \Delta A_\phi - 2 \frac{\partial_r A_\phi}{r} &= 0. \end{aligned} \quad (21)$$

The system of equations (12–20) fully describes disk configurations up to the 1PN order of approximation. It follows from the metric (2) or (4); as we stressed before, both approaches give the same set of equations. Notice that these are integro-differential equations with a free boundary; the shape of a disk comes as a part of the solution. It will be explained in the numerical section, how to deal with such a boundary problem. The second of the equations (21) can cause difficulties for systems with matter located on the z axis; we deal, however, with disks and Eq. (21) is harmless.

The first post-Newtonian correction v_1^ϕ to the angular velocity Ω is obtained from the perturbation expansion of the rotation law (10) up to terms of the order c^{-2} . One arrives at [2]

$$v_1^\phi = -\frac{3}{2}\Omega_0^3 r^2 + \frac{3A_\phi}{4r^2} - 3\Omega_0 h_0. \quad (22)$$

This can be written in a more geometric way. The geometric circumferential radius of the circle $r = \text{const}$, $z = 0$ around the rotation axis is given by $\tilde{r} = r(1 - U_0/c^2) + \mathcal{O}(c^{-4})$. Therefore the angular velocity reads

$$\begin{aligned} \Omega &= \Omega_0 + \frac{v_1^\phi}{c^2} = \frac{w}{\tilde{r}^{3/2}} - \frac{3}{2c^2}\Omega_0 \left(-\frac{m}{\tilde{r}} + U_{0D} + \Omega_0^2 \tilde{r}^2 \right) \\ &\quad + \frac{3A_\phi}{4\tilde{r}^2 c^2} - \frac{3}{c^2}\Omega_0 h_0, \end{aligned} \quad (23)$$

where the last three terms are 1PN corrections. Let us point out that the anti-dragging term $(-\frac{3}{c^2}\Omega_0 h_0)$ is of the opposite sign to the dragging term $\frac{3A_\phi}{4\tilde{r}^2 c^2}$ [1].

IV. CHARACTERISTICS OF THE BLACK HOLE HORIZON

The event horizon coincides, in the stationary case, with the apparent horizon S [18], that is a two-surface S embedded in the 3-hypersurface Σ defined by $t = \text{const}$ such that

$$\begin{aligned} \nabla_i n^i + h_{ij} K^{ij} &= 0, \\ \nabla_i n^i - h_{ij} K^{ij} &> 0. \end{aligned} \quad (24)$$

Here n^i is the unit normal to the surface S , X_i denotes the shift vector, $K_{ij} = \frac{1}{2N} (\nabla_i X_j + \nabla_j X_i)$ is the extrinsic curvature of Σ , $h_{ij} = g_{ij} - n_i n_j$ is the induced metric on S and ∇_i means the covariant derivative on Σ . In our case the shift vector is given by $X_i = (0, 0, -A_\phi/c^3)$. It is easily seen that for the metric (4) the contribution of extrinsic curvature vanishes (albeit some nondiagonal components of K_{ij} are nonzero); thus the apparent horizon becomes a minimal surface. The three-dimensional metric of Σ in spherical coordinates is given by

$$ds_3^2 = (f_-)^4 (dR^2 + R^2 d\theta^2 + R^2 \sin^2 \theta d\phi^2), \quad (25)$$

and we get from the minimal surface equation within Σ

$$\nabla_i n^i = 0. \quad (26)$$

The two-surface S can be assumed to be ϕ -independent, due to the axial symmetry; it is given by the single equation $R = R(\theta)$. Its normal reads

$$n_k = \frac{f_-^2}{\sqrt{1 + \frac{(\partial_\theta R)^2}{R^2}}} (1, -\partial_\theta R, 0). \quad (27)$$

In explicit terms Eq. (26) reads

$$\begin{aligned} \frac{1}{R^2 f_-^6} \partial_R \left[\frac{R^2 f_-^4}{\sqrt{1 + \frac{(\partial_\theta R)^2}{R^2}}} \right] + \\ \frac{1}{\sin \theta R^2 f_-^6} \partial_\theta \left[\frac{\sin \theta (-\partial_\theta R) f_-^4}{\sqrt{1 + \frac{(\partial_\theta R)^2}{R^2}}} \right] = 0. \end{aligned} \quad (28)$$

Equation (28) is a second-order differential equation for the radial function $R(\theta)$. The boundary conditions are given by $\partial_\theta R|_{\theta=0} = \partial_\theta R|_{\theta=\pi} = 0$. Solving of Eq. (28) would be numerically inexpedient, since the 3-metric g_{ij} is known only numerically. Fortunately, numerical results show that the impact of the disk onto the geometry around $R = R_h$ is small. We investigated the behaviour of U_D at R_h for 4 disk configurations with the outer edge at $r_{\text{out}} = 1$ and with the inner edges located at $r_{\text{in}} = 0.1, 0.5, 0.75$ and $r_{\text{in}} = 0.95$. Disk masses exceeded the central mass by a factor of 10. We found that the modulus of the potential U_D depends very weakly on the angle θ and its maximal values are 24.82 (for $r_{\text{in}} = 0.1$),

13.45 (for $r_{\text{in}} = 0.5$), 11.49 (for $r_{\text{in}} = 0.75$) and 10.41 (for $r_{\text{in}} = 0.95$). (See one of later sections for a more detailed description of assumed data.) These values should be compared to the modulus of the central potential m/R_{h} , which gives 2000 (we assumed $m = 1$ in these numerical calculations), that is roughly values larger by 2 orders of magnitude. Thus the potential U_{D} is relatively small and it is almost constant at surfaces $R = \text{const}$; moreover $|\partial_R U_{\text{D}}|/(m/R^2) \approx 0$, in the vicinity of $R_{\text{h}} = m/(2c^2)$.

We believe, basing on the preliminary inspection of Eq. (28), that the following hypothesis is true.

Conjecture. If the disk potential and its derivatives are small,

$$\begin{aligned} \sup_V (|U_{\text{D}}|, |R\partial_R U_{\text{D}}|) &\ll \frac{m}{2R}, \\ \sup_V (|\partial_\theta U_{\text{D}}|, |\partial_\theta^2 U_{\text{D}}|) &\ll \frac{m}{R}, \end{aligned} \quad (29)$$

in a vicinity of $R_{\text{h}} = m/(2c^2)$, then the position of the minimal surface is well approximated by R_{h} .

This Conjecture will be applied later on.

A. The area and mass of minimal surfaces

The metric induced on an axially symmetric two-surface S , that is defined by $R = R(\theta)$, reads

$$ds_{(2)}^2 = f_-^4 R^2 \left[\left(1 + \frac{(\partial_\theta R)^2}{R^2} \right) d\theta^2 + \sin^2 \theta d\phi^2 \right]. \quad (30)$$

The area of the two-surface is given by

$$A_{\text{AH}} = 2\pi \int_0^\pi d\theta R^2 \sin \theta f_-^4 \sqrt{1 + \frac{(\partial_\theta R)^2}{R^2}}. \quad (31)$$

If the 2-surface is minimal and it is located at $R \approx m/(2c^2)$, then the area is approximated by

$$A_{\text{AH}} = \frac{m^2}{2c^4} \pi \int_0^\pi d\theta \sin \theta \left[16 + \frac{16U_{\text{D}}(R, \theta)}{c^2} \right]. \quad (32)$$

In the case of the Schwarzschild black hole one has the strict equality $A_{\text{AH}} = 16\pi \frac{m^2}{c^4}$. The Podurets-Misner-Hawking-Geroch [19] mass of a black hole is defined as $M_{\text{AH}} = c^2 \sqrt{\frac{A_{\text{AH}}}{16\pi}}$, which yields $M_{\text{AH}} = m$ for the Schwarzschild black hole. It is accepted in numerical general relativity as a quasilocal mass measure of horizons in selfgravitating systems [20]. We shall also employ that mass. We will accept only those numerical solutions, where the Podurets-Misner-Hawking-Geroch mass is close to the Newtonian mass m , that is $|m - M_{\text{AH}}(S)| \ll m$ (see Sec. VI). In such a case the mass parameter m still can be interpreted as the mass of the central black hole, and it would be legitimate to use the above Conjecture.

In the 1PN approximation the asymptotic mass of configurations can be read off from the asymptotic behaviour of the superposition of potentials $-\frac{m}{R} + U_{\text{D}}$. As explained above, the parameter m approximates the mass of the central black hole; therefore the asymptotics of U_{D} can be regarded as defining the mass of a rotating disk.

B. The angular momentum

Cylindrically symmetric stationary systems possess a (spatial) Killing vector η^μ , i.e. $\nabla_\mu \eta_\nu + \nabla_\nu \eta_\mu = 0$. The angular momentum of a fluid rotating around the z -axis can be defined as follows [9]

$$\begin{aligned} L &= \frac{1}{c} \int_V t_\mu T_\nu^\mu \eta^\nu dV \\ &= \int_V dr d\phi dz \rho (c^2 + h) \sqrt{-\det g^4} u_\phi u^t. \end{aligned} \quad (33)$$

We use here cylindrical coordinates r, ϕ and z ; t^μ is a normal to the Cauchy hypersurface Σ . The integrand can be expressed as a total divergence (using relevant Einstein equations); applying the Gauss theorem, one can write down the angular momentum as a sum of internal angular momenta, associated to an internal 2-surface S and to the asymptotics [10, 21]: $L = j_S + j_\infty$.

The angular momentum of a surface S , that is defined by $R = R(\theta)$, reads (up to the 1PN approximation)

$$\begin{aligned} j_S &= \int_0^\pi d\theta \frac{R^4}{8} \sin^3 \theta \left(-\partial_R \omega + \frac{\partial_\theta R \partial_\theta \omega}{R^2} \right) \times \\ &\frac{f_-^7}{|f_+|}, \end{aligned} \quad (34)$$

while the asymptotic angular momentum is given by

$$j_\infty = - \int_0^\pi \frac{d\theta}{8} R^4 \sin^3 \theta (-\partial_R \omega). \quad (35)$$

We shall calculate the angular momentum of a minimal surface. Assuming that the above conjecture is valid, that is $R \approx m/(2c^2)$, then $(f_-)^7 \approx 2^7 (1 - 7U_{\text{D}}/(4c^2)) = 128(1 - 7U_{\text{D}}/(4c^2))$ and $|f_+| \approx |U_{\text{D}}|/(2c^2)$. Thus the angular momentum becomes

$$\begin{aligned} j_S &= -16 \int_0^\pi d\theta R^4 \sin^3 \theta \left(\partial_R \omega - \frac{1}{R^2} \partial_\theta R \partial_\theta \omega \right) \times \\ &\frac{1 - 7 \frac{U_{\text{D}}(r, \theta)}{4c^2}}{\frac{|U_{\text{D}}|}{c^2}}. \end{aligned} \quad (36)$$

If the angular dependence of the minimal surface is ‘‘moderate’’, so that terms with $\partial_\theta R$ can be neglected, then taking into account that $|U_{\text{D}}|/c^2 \ll 1$, we get

$$j_S = -16 \int_0^\pi d\theta R^4 \sin^3 \theta \frac{\partial_R \omega}{\frac{|U_{\text{D}}|}{c^2}}. \quad (37)$$

This can be further simplified, since $R \approx m/(2c^2)$. We obtain finally

$$j_S = -\frac{m^4}{c^6} \int_0^\pi d\theta \frac{\sin^3 \theta \partial_R \omega}{|U_D|}. \quad (38)$$

The total angular momentum of a rotating fluid is approximated, up to the 1PN order, by

$$\begin{aligned} L = & \int dr d\phi dz \Omega_0 r^3 \rho_0 + \\ & \frac{1}{c^2} \int dr d\phi dz \rho_0 \left(\Omega_0^3 r^5 - 6\Omega_0 r^3 U + r^3 v_1^\phi - r A_\phi \right) \\ & + \frac{1}{c^2} \int dr d\phi dz (\rho_1 + p_0) r^3 \Omega_0. \end{aligned} \quad (39)$$

The asymptotic value of the angular momentum can be obtained directly or (preferably) from $j_\infty = L - j_S$.

V. DESCRIPTION OF THE NUMERICAL METHOD

The numerical method used in this paper was described in [1]. It is a variant of the old fashioned (but working) Self-Consistent Field (SCF) scheme. The solution representing the disk is found in three stages. In the first one, a strictly Newtonian configuration is obtained. In this stage, each iteration of the SCF method consists in solving the Poisson equation (16) for the gravitational potential and, subsequently, the Euler-Bernoulli equation (15) that yields the specific enthalpy corresponding to a given gravitational potential. The Newtonian solution is parametrized by the values r_{in} and r_{out} of the inner and outer equatorial radii of the disk, respectively — we fix the *coordinate size of the disk*. Further data include the maximum value of the density within the disk, the value of the central mass m , and the polytropic exponent. These parameters allow one to establish the values of the constants K , Ψ_0 , and w in each of the subsequent iterations.

In the second stage we compute the potential A_ϕ , solving Eq. (17). The result depends on previously obtained ρ_0 and Ω_0 .

The third stage is again an iterative one. In each iteration, a post-Newtonian correction U_1 is found by solving Eq. (18). Given the new value of U_1 we obtain the correction to the specific enthalpy h_1 from Eq. (20). There is a degree of freedom in this step that is connected with the choice of constant Ψ_1 in Eq. (20). At the Newtonian stage the analogous constant Ψ_0 is fixed by the geometrical requirement on the size of the disk (setting the inner and outer equatorial radii) and the remaining data (the maximum value of the density, the value of the central mass m , and the polytropic exponent). It seems that at the first post-Newtonian level one can choose the constant Ψ_1 freely. In [1] the value of Ψ_1 was fixed by requiring that the correction to the specific enthalpy h_1 vanishes

at the outermost point of the disk, i.e., at the outer equatorial radius. We found that this choice yields solutions that conform with the post-Newtonian assumptions only in a limited range of parameters. The choice that we employ here is to require that the post-Newtonian correction h_1 (or, equivalently, ρ_1) vanishes at the point where the Newtonian density ρ_0 attains its maximum value. It seems to be a slight change, but it yields acceptable solutions for a much broader range of parameters. *This fact probably conveys an important message, that in this kind of general-relativistic free boundary problems, that we are dealing with, the maximal (baryonic) mass density should always be a part of given data.* Note also that the apparent freedom of choosing the value of the constant Ψ_1 is yet another manifestation of the non-uniqueness of the post-Newtonian expansion with respect to stationary systems [2].

In summary, we adopted following input data: the coordinates of the inner and outer boundaries of the disk, the maximal mass density, and a *functional form* of the rotation law and of the equation of state. That is, we assume $p = K\rho^\gamma$, but the specific value of the coefficient K is a part of a solution. Similarly, the parameters w and Ψ in the rotation law — see Eq. (10) — are established after finding the Newtonian (or 1PN) disk configuration.

Technical aspects of our numerical method are quite standard; they are described in [1]. We work in spherical coordinates (R, θ, ϕ) . For convenience we also define $\mu = \cos \theta$. Equations (16), (17) and (18) are solved using appropriate Green functions that are expanded in Legendre polynomials.

Equations (16) and (18) have the form of a Poisson equation $\Delta\Phi = f(R, \mu)$ that has to be solved assuming that the solution vanishes at infinity. We compute the solution Φ as

$$\Phi(R, \mu) = -\frac{1}{2} \sum_{j=0}^N P_j(\mu) \left[\frac{1}{R^{j+1}} E_j(R) + R^j F_j(R) \right], \quad (40)$$

where

$$E_j(R) = \int_0^R dR' R'^{j+2} \int_{-1}^1 d\mu' P_j(\mu') f(R', \mu'), \quad (41)$$

$$F_j(R) = \int_R^\infty dR' \frac{1}{R'^{j-1}} \int_{-1}^1 d\mu' P_j(\mu') f(R', \mu'). \quad (42)$$

Equation (17) has the form

$$\Delta A_\phi - \frac{2\partial_r A_\phi}{r} = g(R, \mu), \quad (43)$$

which is directly related to the vectorial Poisson equation (cf. [1]). The solution A_ϕ that vanishes at infinity can be found as

$$A_\phi(R, \mu) = -\frac{1}{2} \sqrt{1 - \mu^2} \sum_{j=1}^N \frac{1}{j(j+1)} P_j^1(\mu)$$

$$\left[\frac{1}{R^j} C_j(R) + R^{j+1} D_j(R) \right], \quad (44)$$

where

$$C_j(R) = \int_0^R dR' R'^{j+1} \int_{-1}^1 \frac{d\mu'}{\sqrt{1-\mu'^2}} P_j^1(\mu') g(R', \mu'), \quad (45)$$

$$D_j(R) = \int_R^\infty dR' \frac{1}{R'^j} \int_{-1}^1 \frac{d\mu'}{\sqrt{1-\mu'^2}} P_j^1(\mu') g(R', \mu'). \quad (46)$$

Symbols P_j and P_j^1 denote Legendre polynomials and associated Legendre polynomials of the first order, respectively. Assuming equatorial symmetry one can show that all above integrals with P_{2j+1} and P_{2j}^1 , $j = 0, 1, 2, \dots$ vanish.

The above formulae are exact for $N \rightarrow \infty$. In our applications we set $N \approx 100$. The integrals are computed on a spherical grid assuming a piecewise linear interpolation of $f(R, \mu)$ and $g(R, \mu)$. In most cases, the resulting integrals can be then computed analytically. Otherwise Simpson's rule is used.

The last ingredient of the numerical method is directly related to the fact that we are dealing with the free-boundary problem. In the first stage — at the Newtonian level — one ensures that no negative values of h_0 appear in the solution. At all grid points where Eq. (20) yields a negative value of h_0 we set $h_0 = 0$. This defines the shape of the disk at each iteration step.

A similar procedure has to be implemented at the 1PN stage. The cutoff is applied to ρ_1 . Whenever $\rho_0 + \rho_1/c^2$ would become negative, we set $\rho_1 = -c^2\rho_0$. Note that, in practice, corrections ρ_1 and h_1 are related by

$$\rho_1 = \frac{1}{K^\gamma} \rho_0^{2-\gamma} h_1. \quad (47)$$

Thus $\rho_0 = 0$ implies $\rho_1 = 0$ provided that h_1 remains finite.

We use a numerical grid consisting of 200 zones in the radial direction and 800 zones in the angular one. It is important to note that disks which are relatively light in comparison to the central mass (i.e., $M_D \ll m$) become slim. Consequently, it is crucial to provide sufficient angular resolution also in those cases. In a general case, our grid covers in the angular direction the region $0 \leq \mu \leq 1$. For thin disks we confine ourselves to $0 \leq \mu \leq 1/2$ or even $0 \leq \mu \leq 1/10$, keeping the same number of 800 angular zones. For example, for an elongated disk with $r_{\text{in}}/r_{\text{out}} = 1/10$ and $M_D/m \approx 10^{-4}$ we get the maximal height of the disk above the symmetry plane $z = 0$, $h_{\text{max}} \approx 0.01r_{\text{out}}$. In our setup this corresponds to approximately 100 angular zones occupied by the disk. This procedure was also tested for the purely Newtonian case in [23], where a disk with a relative thickness of the order of 1/1000 was computed, using up to $L = 400$ Legendre polynomials and numerical grids spanning up to 5000×5000 nodes.

To some extent, the correctness of our numerical procedure can be tested by computing suitable virial identities. Such identities were derived in [22]. In [22] we also provided examples of convergence tests of our numerical method.

VI. NUMERICS: MASS RATIO AND DRAGGING OF ROTATING SYSTEMS

A. Introductory remarks

We show in this section that maximal values of the total dragging and its constituents simply scale with the total mass, up to the 1PN order. We define normalized post-Newtonian corrections: the total $S_T \equiv |v_1^\phi/(c^2\Omega_0)|$ (see (22)) correction and its constituent components — the dragging (geometric) term $S_g \equiv |\frac{3A_\phi}{4\bar{r}^2\Omega_0 c^2}|$, the anti-dragging term $S_{\text{ad}} \equiv |\frac{3h_0}{c^2}|$ and the centrifugal term $S_c \equiv |\frac{3}{2c^2}(-\frac{m}{R} + U_{0D} + \Omega_0^2 r^2)|$. It will appear that their maximal values almost linearly depend on the mass functional M_D . We take care to ensure that the calculation is done well within the post-Newtonian regime: the modulus of the 1PN correction to the metric within tori, $2|U|/c^2$, is usually smaller (or much smaller) than 0.01 and reaches 0.05 only for heaviest disks.

We assume in the numerical analysis that maximal values of S_T , S_g , S_{ad} and S_c can occur only at the equatorial plane $z = 0$. These functions satisfy elliptic equations; see (17) for the equation for A_ϕ , take into account that $S_{\text{ad}} \propto h_0$ and notice that S_c is a linear function of the enthalpy density h_0 (see (15)). The function h_0 satisfies equation

$$\Delta h_0 = -4\pi\rho_0 - \Omega_0^2 r. \quad (48)$$

We believe that by invoking the maximum (minimum) principle — specifically, the moving planes method [24] — one can prove that maximal points exist at $z = 0$.

Taking that into account, and exploiting the axial symmetry, one would need to find the maximal values of S_T , S_g , S_{ad} and S_c in the line interval $(r_{\text{in}}, r_{\text{out}})$ within the equatorial section of the disk. That is a formidable but feasible numerical task.

We shall investigate disks extending from the innermost equatorial circle corresponding to $r_{\text{in}} = 0.1, 0.4, 0.5, 0.6, 0.75$ and 0.95 to the outermost equatorial circle $r_{\text{out}} = 1$. The results are comprised in 10 diagrams and 2 tables — each of graphs demanded at least 2 dozens of numerical solutions.

It is useful to translate coordinate distances onto geometric ones, using R_S , the Schwarzschild radius of the central black hole. It is assumed in all numerical calculations that the central mass is equal to 1 and the speed of light is such that $c^2 = 1000$. The distance areal scale is thus defined by its Schwarzschild radius $R_S = 2/c^2 = 1/500$, that corresponds to the isotropic coordinate radius $R = 1/2000$. We constructed our toroids

in limits of the 1PN order of approximation, which means that conformal factors f (see the metric (4)) are close to unity within the volumes of toroids. Thus the areal radius of the innermost equatorial circle r_{in} is given by $R(r_{\text{in}}) = r_{\text{in}} f^2(r_{\text{in}}) \approx r_{\text{in}}$. Therefore inner areal radii of investigated toroids change from about 50 times R_S (for $r_{\text{in}} = 0.1$) to $475R_S$ (for $r_{\text{in}} = 0.95$). The coordinate boundary of the whole system is located at $r_{\text{out}} = 1$ and that corresponds to the areal size of (approximately) $500R_S$.

We observe that the geometric contribution $\text{sup } S_g$ to the total dragging is essentially independent of the distance of the disk from the central black hole: $\text{sup } S_g = \beta M_D/m$, where the proportionality coefficient β depends weakly only on the ratio M_D/m and $\beta \in (0.2, 0.5) \times 10^{-3}$.

The anti-dragging $\text{sup } S_{\text{ad}}$ and centrifugal $\text{sup } S_c$ terms strongly depend on the disk's distance from the black hole; they dominate at distances of the order of $50R_S$ and are dwarfed by the geometric dragging effect represented by $\text{sup } S_g$ at the distance of $300R_S$.

B. Partial dragging effects

In Figs. 1–3 we plot the dependence of the maximal value of the normalized dragging, anti-dragging and centrifugal 1PN corrections on the relative mass M_D/m . The equation of state is $p = K\rho^{4/3}$. There are a few dozens of solutions corresponding to each of the three systems with the inner radii r_{in} situated at 0.1, 0.4 and 0.6. Numerical data suggest that the quantities $\text{sup } S_g$, $\text{sup } S_{\text{ad}}$ and $\text{sup } S_c$ are linear functions of the relative mass M_D/m . We display the results in three diagrams. In Fig. 1 the ratio M_D/m is smaller than 0.001, in Fig. 2 we have $M_D/m < 1$ while in Fig. 3 the disk mass changes between 0 and 40 of the central mass. In each case there is an approximately linear behaviour.

We observe that the slope coefficient of the geometric dragging quantity $\text{sup } S_g/M_D$ is only weakly dependent on the position of a disk — it changes slightly with the change of the inner radius r_{in} . In contrast to that, the slopes of the anti-dragging and centrifugal objects $\text{sup } S_{\text{ad}}/M_D$ and $\text{sup } S_c/M_D$ are quite sensitive to the disk location; they become significantly smaller with the increasing distance from the central black hole. For the case $r_{\text{in}} = 0.1$ we have $\text{sup } S_{\text{ad}} > \text{sup } S_c > \text{sup } S_g$; clearly the anti-dragging effect dominates, for all masses within the range $M_D \in (10^{-4}m, 40m)$. With the increase of the distance the picture reverses; at $r_{\text{in}} = 0.6$ we have $\text{sup } S_g > \text{sup } S_c > \text{sup } S_{\text{ad}}$. One can notice, choosing two disks of the same mass but with different inner boundaries, that the value of $\text{sup } S_{\text{ad}}$ at $r_{\text{in}} = 0.6$ is about one half of its value at $r_{\text{in}} = 0.1$.

One can read from these diagrams, that for the equation of state $p = K\rho^{4/3}$ and $M_D < 10^{-3}m$, the correction $\text{sup } S_g \approx 4 \times 10^{-3} M_D/m$ (see Fig. 1); the same equation of state corresponds to $\text{sup } S_g \approx (2.8 - 3.2) \times 10^{-3} M_D/m$, where $M_D \in (m, 40m)$ (see Fig. 3).

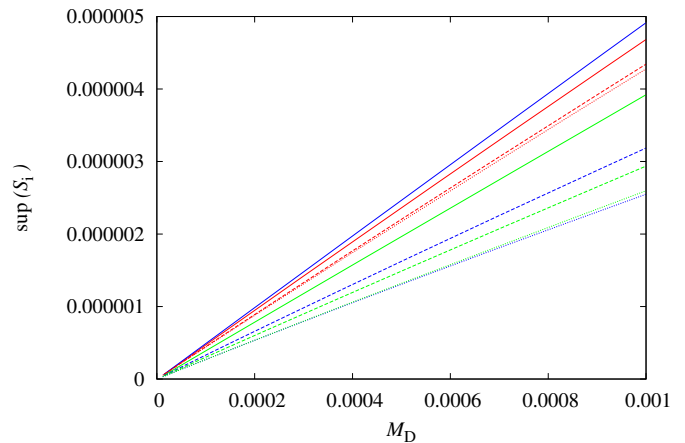


FIG. 1. The normalized 1PN corrections $\text{sup } S_g$ (red lines), $\text{sup } S_{\text{ad}}$ (blue lines) and $\text{sup } S_c$ (green lines), within the symmetry plane of the disk, put on the vertical axis — in function of the mass ratio $M_D/m \leq 0.001$ (displayed on the abscissa). The inner disks's boundaries are located at $r_{\text{in}} = 0.1$ (solid lines), 0.4 (broken lines) and 0.6 (dotted lines), respectively. The equation of state $p = K\rho^{4/3}$.

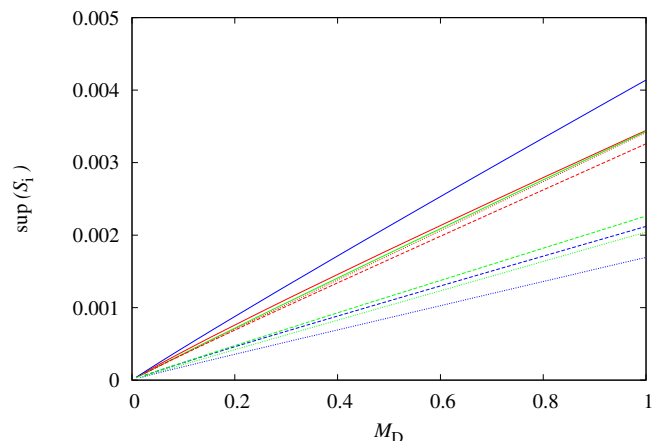


FIG. 2. The same as in Fig. 1, but with disk masses in the interval $(0, m)$.

This analysis yields similar results also for disks with the polytropic equation of state $p = K\rho^{5/3}$ (see Figs. 4–6), with several notable differences. In the mass interval $M \in (0, 10^{-3})m$ and $r_{\text{in}} = 0.1$ we observe $S_g > S_c > S_{\text{ad}}$, while the centrifugal term $\text{sup } S_c$ dominates at $r_{\text{in}} = 0.1$ for higher disk masses. The anti-dragging related object $\text{sup } S_{\text{ad}}$ exceeds the geometric part $\text{sup } S_g$ only for $M_D > 0.4m$, again only at $r_{\text{in}} = 0.1$. When $r_{\text{in}} = 0.4$ or 0.6 , then always geometric effects dominate over centrifugal ones, and those anti-dragging ones are the weakest of all.

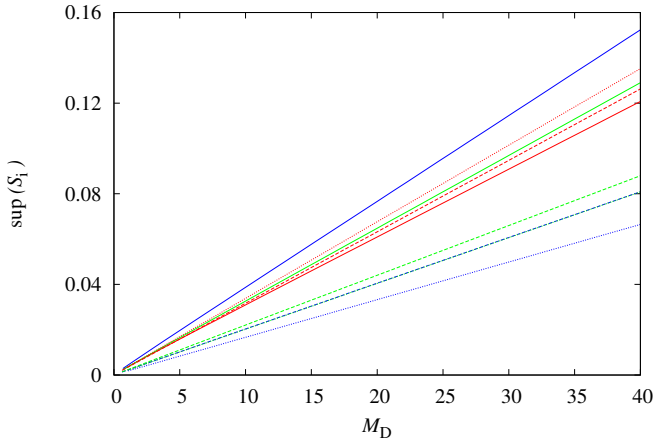


FIG. 3. The same as in Fig. 1, but with disk masses in the interval $(m, 40m)$.

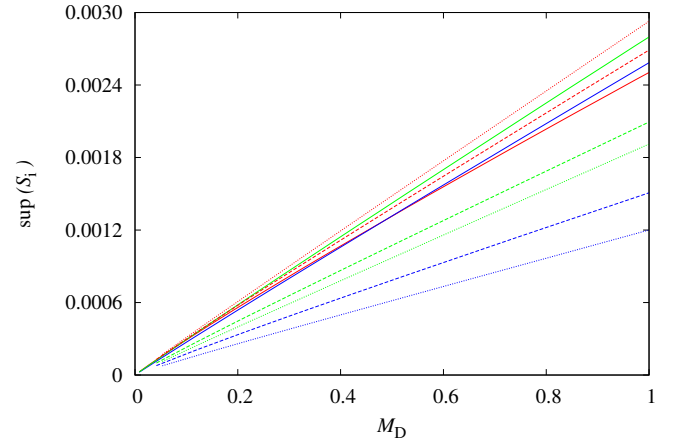


FIG. 5. The same as in Fig. 4, but with disk masses in the interval $(0, m)$.

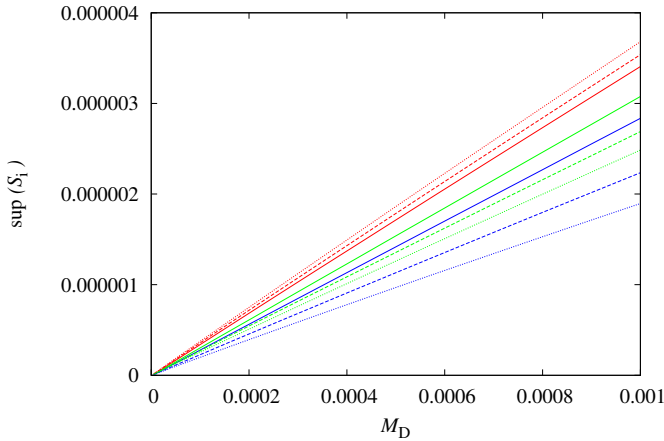


FIG. 4. The normalized 1PN corrections $\sup S_g$ (red lines), $\sup S_{ad}$ (blue lines) and $\sup S_c$ (green lines), within the symmetry plane of the disk, put on the ordinate — in function of the mass ratio $M_D/m \leq 0.001$ (displayed on the abscissa). The inner disks's boundaries located at $r_{in} = 0.1$ (solid lines), 0.4 (broken lines) and 0.6 (dotted lines), respectively. The equation of state is $p = K\rho^{5/3}$.

C. Total dragging: a linear function of relative mass

In Figs. 7 and 8 we plot the dependence of the maximal value of the normalized 1PN correction $S_T = \frac{v_1^\phi}{\Omega_0 c^2}$ on the relative mass M_D/m .

We have found several dozens of solutions corresponding to each of the four systems with the inner radii r_{in} situated at $0.1, 0.5, 0.75$ and 0.95 . Again it appears that $\sup S_T$ is a strictly linear function of the relative mass. For the sake of clarity, we show corresponding results

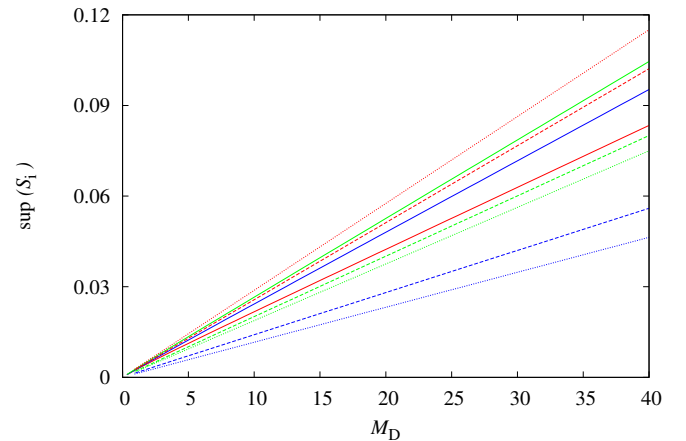


FIG. 6. The same as in Fig. 4, but with disk masses in the interval $(m, 40m)$.

in two diagrams. In Fig. 7, for the equation of state $p = K\rho^{4/3}$, the mass of the disk is smaller than $5m$. The most interesting feature of these plots is that the steepest line correspond to the farthest disk; for a fixed mass of disks the maximal value of the normalized correction S_T increases with the increase of r_{in} .

In Fig. 8, which corresponds to the equation of state $p = K\rho^{5/3}$, the disk mass changes between 0 and $20m$. The steepness of the lines is almost the same as in the Fig. 7, and again the steepest lines correspond to the farthest disk.

A closer inspection in the regime of light disks, with masses significantly smaller than the central mass, reveals a more complex picture (see Fig. 9). For light disks — our rough estimate is $M_D < 0.2m$ — the normalized dragging $\sup S_T$ for disks with inner boundaries located

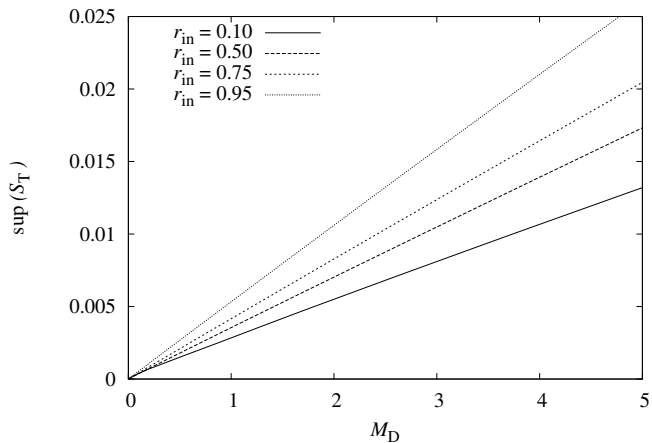


FIG. 7. The maximum of the normalized 1PN correction $\frac{v_{\phi}^2}{\Omega_0 c^2}$ within the disk (on the ordinate) in function of the asymptotic mass of the disk M_D (plotted on the abscissa), for disks with inner boundaries located at $r_{\text{in}} = 0.1, 0.5, 0.75$ and 0.95 , respectively. The equation of state is $p = K\rho^{4/3}$.

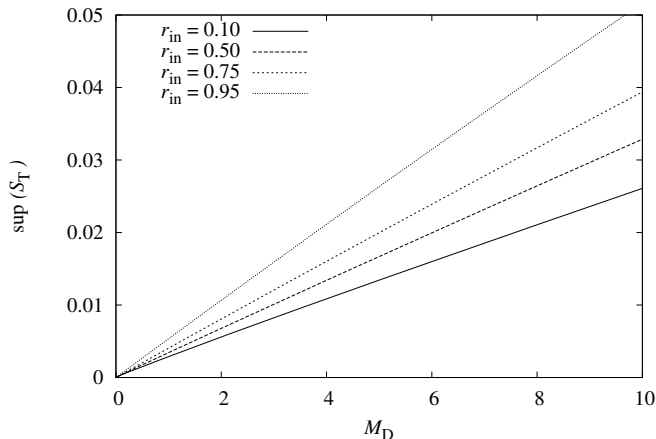


FIG. 8. The same as in Fig. 7, but for the equation of state $p = K\rho^{5/3}$.

at r_{in} may decrease with the increase of r_{in} , and then it can start to increase. The value of the critical radius r_{cr} , where the behaviour changes, depends on the mass M_D , but is probably smaller than half of the central mass. In the situation displayed on Fig. 9, we observe that $\text{sup } S_T(r_{\text{in}} = 0.1)$ (solid line) intersects with $\text{sup } S_T(r_{\text{in}} = 0.5)$ (long broken line), at masses (roughly) $0.01 m$ and $0.12 m$. That means that disks with masses in the interval $(0.01m, 0.12m)$ are characterized by functions $\text{sup } S_T$ that are not monotonic as functions of r_{in} , in the region $0.1 < r_{\text{in}} < 0.5$.

This behaviour is due to the rapid growth of the anti-dragging term $\text{sup } S_{\text{ad}}$ with the increase of mass that

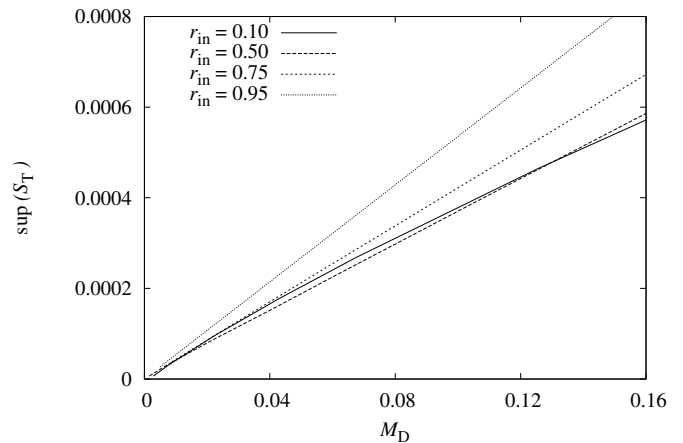


FIG. 9. The values of $\text{sup } S_T$ are put on ordinate, while disk masses are put on the abscissa. The two lines corresponding to $r_{\text{in}} = 0.1$ (solid line) and $r_{\text{in}} = 0.5$ (broken line) cross around $M_D = 0.11m$. The equation of state is $K\rho^{4/3}$.

compensates a moderate growth of the dragging quantity $\text{sup } S_g$ (compare Figs. 1 and 2), for disk masses that are small enough. That would cause the falloff of the normalized correction $\text{sup } S_T$ in an interval of small radii r_{in} .

VII. ANGULAR MOMENTUM: LOCAL VERSUS TOTAL

In this section we address issues concerning the dragging at the black hole horizon and the distribution of angular momentum in systems with rotating rings. Let us recall that Nishida and Eriguchi [3] applied the rotation law $j(\Omega) = A(\Omega - B)$. They found, in particular, that the angular momentum of the central black hole can vanish and — more generally — its internal spinning parameter a_S can be both negative and positive. For some configurations one would have $|a_S| > 1$ and the dragging function A_ϕ would vanish at the horizon. Ansorg and Petroff [4] assumed the constant angular velocity within the disk and they also obtained central black holes with $|a_S| > 1$.

Our results are comprised in Table 1. The internal spinning parameter a_S is contained within the range $(10^{-4}, 10^{-10})$. That means that the central black hole can be safely approximated by a Schwarzschild black hole. We already proved that the metric function A_ϕ can have only isolated zeroes [1]; that is, it cannot vanish at the horizon of the black hole. There is an apparent discrepancy between our results and those of [3–5]. This can be ascribed mainly to the fact, that our central black hole is inherently spinless, in contrast to what was assumed in quoted papers, in which central black holes possessed their own internal spin. We think, however, that a differ-

ent choice of the rotation law — the uniform rotation [4], the constant j adopted by Shibata [5] and the linear law $j(\Omega) = A(\Omega - B)$ [3], within the fully general-relativistic equilibrium — instead of the Keplerian rotation law (9) in the perturbation equilibrium (up to the 1PN order) — also played a role. It might happen that for the post-Newtonian descriptions with $\Omega = \text{const}$ or $j = \text{const}$ the apparent horizon's spinning parameter would be much larger than observed here. We cannot exclude also that the fully general-relativistic equilibria with the Keplerian law (9) would have values of a_S exceeding 1.

Figure 10 shows the dimensionless spinning parameter for the whole spacetime, $a_\infty \equiv \frac{cJ_\infty}{M^2}$, where M is the total mass read off from the asymptotic behaviour of the total potential $-\frac{m}{R} + U_D$. Let us remark that for the Schwarzschild black hole $a_\infty = 0$, while for the extremal Kerr black hole $a_\infty = 1$. All nonextremal Kerr black holes have $0 < a_\infty < 1$. In our case we have values of a_∞ that are large for disks heavier than the black hole and that are small in the opposite case, when $M_D \ll m$. Our numerical data clearly demonstrate that the spinning parameter in non-Kerr stationary configurations can be significantly larger than 1.

The most significant observation is that only a tiny fraction j_S of the angular momentum is deposited within the central black hole. The ratio j_S/j_∞ varies from 10^{-6} for the disk closest to the center, with the equatorial inner edge located at $r_{\text{in}} = 0.1$ (which corresponds to about 50 R_S) to 10^{-12} for systems with the equatorial inner edge placed at $r_{\text{in}} = 0.95$ (that corresponds to about 475 R_S).

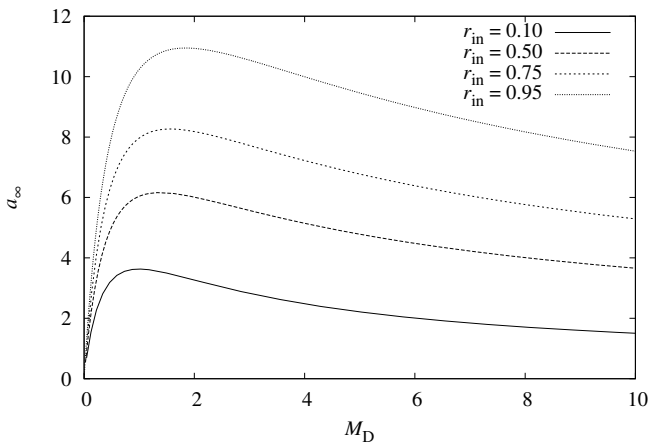


FIG. 10. Asymptotic values of the spin parameter $a_\infty \equiv \frac{cJ_\infty}{M^2}$, where $M = m + M_D$ is the asymptotic mass.

VIII. ANGULAR MOMENTUM AND ISOPERIMETRIC INEQUALITIES

We shall start with a compendium on various concepts of mass and mass densities. In formula (3) appears the

TABLE I. The asymptotic angular momentum (the first column) and the black hole angular momentum for disks with $r_{\text{in}} = 0.1$ (the third column). Fourth column gives the disks's mass in units of the central mass m . The second column displays the area of the central black hole in terms of $R_S \equiv 2m/c^2$. The last column is the maximal height of the disk.

L	$A_{\text{AH}}/16\pi$	j_S	M_D	h_{max}
0.6880	0.9972	6.034×10^{-10}	1.493	0.3922
1.006	0.9959	1.339×10^{-10}	2.156	0.3922
1.351	0.9945	2.459×10^{-9}	2.848	0.4269
1.723	0.9931	4.018×10^{-9}	3.561	0.4529
2.119	0.9917	6.065×10^{-9}	4.290	0.4728
2.539	0.9903	8.644×10^{-9}	5.032	0.4883
2.981	0.9888	1.180×10^{-8}	5.783	0.5012
3.445	0.9873	1.557×10^{-8}	6.544	0.5120
6.071	0.9798	4.543×10^{-8}	10.43	0.5211
9.174	0.9722	9.539×10^{-8}	14.42	0.5515
12.72	0.9645	1.709×10^{-7}	18.50	0.5688
16.70	0.9568	2.755×10^{-7}	22.64	0.5799
21.09	0.9490	4.134×10^{-7}	26.84	0.5878
25.89	0.9413	5.886×10^{-7}	31.11	0.5935
31.08	0.9335	8.051×10^{-7}	35.43	0.6014
36.67	0.9258	1.067×10^{-6}	39.82	0.6044

baryonic mass density ρ . It plays the role of an integration factor, ensuring the conservation of the baryonic current ρu^μ : $\nabla_\mu(\rho u^\mu) = 0$. The volume integral $\int_V dV \rho$ is the baryonic mass — a quantity that is conserved. In the Newtonian limit the baryonic mass coincides with asymptotic mass, but within General Relativity the asymptotic (Bondi-Einstein-Landau-Lifschitz-Freund-Trautman-Arnowitz-Deser-Misner) mass (see [25] for a discussion) is distinct from the baryonic mass. In our foregoing considerations we always dealt with the conserved (ADM) asymptotic mass. One defines also the rest energy density $e \equiv \rho(c^2 + h) - p = \rho c^2 + \frac{p}{\gamma-1}$, the total rest energy $E_r \equiv \int_V dV e$ [26] and the related rest mass $M_r(V) \equiv \frac{1}{c^2} \int_V dV e$ (see, for instance, [26]).

One defines the momentum density $J_\nu \equiv t_\mu T_\nu^\mu$. It is well known that perfect fluids with the polytropic exponent $\gamma \leq 2$ satisfy the dominant energy condition $e \geq \sqrt{J^k J_k} \equiv |J|$ [18], that reduces in our case to the inequality

$$e \geq \sqrt{J^\phi J_\phi}. \quad (49)$$

It was already shown that — assuming the dominant energy condition, conformal flatness and a kind of convexity — the total rest mass $M_r(V)$ can be bounded by $2c^2 l(V)$, where l is a geodesic size of the configuration [27–32]. These are special cases, but they are in a sense more general than it is needed for our purpose, since their derivation does not require the assumption of stationar-

ity, adopted in this paper; it is enough to guarantee that the configurations are momentarily static. On the other hand, one needs a regular center and a kind of convexity, that can be obeyed by rotating stars, but which is not valid for rotating toroids. Thus application of estimates of the type

$$M_r(V) \leq 2c^2 l(V) \quad (50)$$

— bounding the rest mass in terms of geodesic radii — to toroidal systems would require a renewed analysis.

Dain recently investigated two other size measures, related to the so-called radius R_{SY} of Schoen and Yau [33]. One of them is defined as

$$R' \equiv \frac{2\sqrt{\int_V |\eta| dV}}{\pi R_{\text{SY}}} \quad (51)$$

while the other is given by

$$\hat{R} \equiv \frac{2\sqrt{\int_V |\eta| dV}}{\pi R_{\text{OM}}}; \quad (52)$$

here R_{OM} is a modification of the R_{SY} measure due to N. Ó Murchadha [34]. They are formulated in terms of quantities relating entirely to toroids; they do not assume convexity and they can be applied to systems investigated in this paper.

The total angular momentum can be written as $L = c^{-1} \int_V J_\nu \eta^\nu dV = c^{-1} \int_V J_\phi dV$. The application of (49) to the definition of the angular momentum (33) gives a string of inequalities

$$\begin{aligned} |L| &\leq \frac{1}{c} \int_V |J| |\eta| dV \leq \frac{1}{c} \sup_V |\eta| \int_V |J| dV \\ &\leq c \sup_V |\eta| M_r(V). \end{aligned} \quad (53)$$

In the last inequality, we have used the assumption that the data satisfy the dominant energy condition. Provided that $M_r(V) \leq 2c^2 l(V)$ and that we are in the perturbative regime (which means that the conformal factor is close to 1, we get $\sup_V |\eta| \approx R(V)$, where $R(V) = C/(2\pi)$ is the areal size of a toroid; its circumference C divided by 2π . This leads to the inequality, that is valid for rotating toroids, supposing conformal flatness and the perturbative regime,

$$|L_z| \lesssim 2c^3 R(V) l(V). \quad (54)$$

This derivation of (54) is analogous to that of S. Dain [6, 7] for axially symmetric systems, without postulating stationarity, but assuming an isoperimetric inequality as in (50).

Dain has got another bound onto a local angular momentum within a finite volume, that does not require postulating any isoperimetric inequalities but instead assumes constant density bodies, of the form

$$\hat{R}^2 \geq \delta \frac{1}{c^3} |L| \quad (55)$$

Here $\delta = \frac{24}{\pi^3}$ is a coefficient of the order of unity and $\hat{R} = \hat{R}$ or $\hat{R} = R'$. We have to note that, unfortunately, rotating disks are not characterized by constant mass densities.

M. Khuri obtained a similar upper bound, dropping the assumption of constant density but imposing a stronger energy condition and a strong un-trapped condition [35].

Tables I and II show results of our numerical calculations. Columns 1 and 3 show values of angular momentum of the whole system and of the black hole, respectively; clearly, the angular momentum deposits in peripheral regions. Column 2 shows values of the control parameter $c_p \equiv \frac{\int_S d^2 S}{4\pi R_S^2}$; all its entries should be close to 1, since that means that the horizon is indeed located at the coordinate radius $R \approx \frac{m}{2c^2}$, as assumed in the numerical calculation. Column 4 shows the mass of the disk in terms of the central mass m . The last column presents the coordinate height of the disk. Let us remind that we assumed $c^2 = 1000$.

The validity of (54) is expected, since it can be proven in the 1PN order of approximation, but the fact that it is satisfied with a huge margin may be interpreted as suggesting the universality of the isoperimetric inequality (50).

The geometry inside toroids is approximately Euclidean, hence the Schoen and Yau radius R_{SY} is roughly equal to one half of the $\min(\frac{1}{2}(r_{\text{out}} - r_{\text{in}}), h)$; it is easy to check that $R_{\text{SY}}^2 \gg \frac{1}{c^3} |L|$ for all systems that are described in Table I, while $R_{\text{SY}}^2 \ll \frac{1}{c^3} |L|$ for configurations listed in Table II. Both measures R' and \hat{R} are much greater than R_{SY} (they are of the order of $R(V)$, or of the radius of the great circle of the toroid) and the inequality (55) holds true for both of them, and for all systems displayed in the two Tables. That might be regarded as surprising, since — as we pointed above — stationary selfgravitating toroids do not satisfy the basic condition of [6], that the mass density is constant; that probably means that a better analytic estimate should be available under much weaker suppositions.

IX. CONCLUDING REMARKS

We have demonstrated, that in Keplerian systems consisting of a rotating toroid and a *spinless* black hole, the black hole can be (essentially) Schwarzschildian — almost all angular momentum is deposited within the toroid. This is true for a large spectrum of systems, for disk masses $M_D \in (10^{-4}m, 40m)$ (m is the black hole mass). That observation would mean, that there is a need to do a more careful interpretation of those astrophysical objects with black holes where the Keplerian rotation curve is observed. The standard practise is to assume that the black hole is Kerr-like and that the toroid is test-like, that is its self-gravity can be neglected. Our results suggest that an alternative picture is plausible, with the central black hole being Schwarzschildian and

TABLE II. The asymptotic angular momentum (the first column) and the black hole angular momentum for disks with $r_{\text{in}} = 0.95$ (the third column). Fourth column gives the disks's mass in units of the central mass m . The second column depicts the area of the central black hole radius in terms of $R_{\text{S}} \equiv 2m/c^2$. The last column is the maximal height of the disk.

L	$A_{\text{AH}}/16\pi$	j_{S}	M_{D}	h_{max}
1.530	0.9988	4.176×10^{-11}	1.145	0.033391
2.563	0.9983	1.048×10^{-10}	1.722	0.033395
3.775	0.9977	2.037×10^{-10}	2.302	0.033395
5.061	0.9971	3.435×10^{-10}	2.885	0.033395
6.503	0.9965	5.287×10^{-10}	3.470	0.033395
8.062	0.9959	7.632×10^{-10}	4.059	0.033395
9.733	0.9953	1.051×10^{-9}	4.650	0.033395
11.15	0.9947	1.396×10^{-9}	5.243	0.033395
13.39	0.9942	1.800×10^{-9}	5.839	0.033395
15.37	0.9936	2.269×10^{-9}	6.438	0.033395
17.45	0.9930	2.804×10^{-9}	7.040	0.033395
19.62	0.9924	3.409×10^{-9}	7.645	0.033395
21.88	0.9918	4.086×10^{-9}	8.252	0.033395
24.23	0.9912	4.839×10^{-9}	8.862	0.033395
26.67	0.9906	5.670×10^{-9}	9.474	0.033395
29.20	0.9901	6.583×10^{-9}	10.09	0.033395
31.81	0.9895	7.579×10^{-9}	10.70	0.033395
34.50	0.9889	8.661×10^{-9}	11.33	0.033395
37.28	0.9883	9.832×10^{-9}	11.95	0.033395

the disk carrying angular momentum and selfgravitating, even for light disks, $M_{\text{D}}/m \ll 1$.

Our numerics suggests that there is a need to include the all *three* weak field components of the general-relativistic effects [2] in gaseous disks circulating around a spinless black hole. The geometric (frame-dragging) effect becomes dominating at relatively large distances; the two other effects can contribute up to 50% even at distances $R \approx 500R_{\text{S}}$, and even for light disks, $M_{\text{D}} \ll m$.

One of the main surprises in this investigation is the fact, that all weak general-relativistic components (dragging, anti-dragging and the centrifugal) scale with M_{D}/m ; their maximal values are proportional to M_{D}/m .

The same is true concerning the total 1PN correction to the angular velocity. We do not know any simple explanation of that fact. Why a fairly complicated normalized post-Newtonian correction S_{T} or its normalized compounds: dragging S_{g} , anti-dragging S_{ad} and centrifugal S_{c} should have maximal values that almost linearly depend on the mass functional M_{D} ? This scaling would mean that the Dopplerian width of spectral lines, of general-relativistic origin, emitted by sources corotating with Keplerian stationary disks scales proportionately to M_{D}/m . This opens, in principle at least, a new observational method for estimating masses in such objects.

The mathematical problems related to stationary rotating polytropes are known as free boundary problems. There are numerical approaches that might inspire the future mathematics of such systems; we should mention here the pioneering work of Hachisu [36], Eriguchi and Nishida [21] and others [37]. They are analysed — with emphasis on the convergence of the SCF approaches — in the recent work of Price, Markakis and Friedman [38]. Hachisu [36] pointed out the necessity to include the maximal value of the fluid mass density, for rotating newtonian polytropes, in the catalogue of assumed data for the self-consistent field method. Our work brings a new technical element — that the maximal (baryonic) mass density should be a part of given data (at least up to the 1PN order), in addition to the rotation law, the equation of state and information on spatial extendibility. Little is known about mathematical setting of rotating selfgravitating systems within general relativity.

Finally, we confirmed the validity of estimates formulated by S. Dain [6]. They imply, in particular, that the angular momentum is located mostly in peripherals of rotating black-hole-toroidal systems; this is consistent with the numerical results reported above.

ACKNOWLEDGMENTS

N. Xie is partially supported by the National Science Foundation of China No.11421061. This research was carried out with the supercomputer “Deszno” purchased thanks to the financial support of the European Regional Development Fund in the framework of the Polish Innovation Economy Operational Program (contract no. POIG. 02.01.00-12-023/08).

[1] P. Jaranowski, P. Mach, E. Malec and M. Piróg, Phys. Rev. **D91**, 024039 (2015).
[2] P. Mach and E. Malec, Phys. Rev. **D91**, 124053 (2015).
[3] S. Nishida and Y. Eriguchi, Astrophys. J. **427**, 429 (1994).
[4] M. Ansorg and D. Petroff, Phys. Rev. **D72**, 024019 (2005).
[5] M. Shibata, Phys. Rev. **D76**, 064035 (2007).
[6] S. Dain, Phys. Rev. Lett. **112** 041101 (2014).

[7] S. Dain, Gen. Rel. Grav. **46**, 1715 (2014).
[8] M. Shibata, Phys. Rev. **D55**, 6019 (1997).
[9] L. G. Fishbone and V. Moncrief, Astrophys. J. **207**, 962 (1976).
[10] J. M. Bardeen, in Black Holes, ed. C. DeWitt and B. S. DeWitt, New York: Gordon and Breach, 1973.
[11] J. M. Bardeen, Astrophys. J. **162**, 71 (1970).
[12] E. Butterworth and I. Ipser, Astrophys. J. **200**, L103 (1969).

- [13] S. Nishida, Y. Eriguchi and A. Lanza, *Astrophys. J.* **401**, 618 (1992).
- [14] F. Galeazzi, S. Yoshida and Y. Eriguchi, *Astronomy and Astrophysics* **541**, 156 (2012).
- [15] K. Uryu, A. Tsokaros, F. Galeazzi, H. Hotta, M. Sugimura, K. Taniguchi and S. Yoshida, *Phys. Rev.* **D93**, 044056 (2016).
- [16] L. Blanchet, T. Damour, and G. Schäfer, *Mon. Not. R. Astron. Soc.* **242**, 289 (1990).
- [17] P. Mach, E. Malec and M. Piróg, *Acta Phys. Pol.* **B44**, 107 (2013).
- [18] R. Wald, *General Relativity*, Chicago: Univ. of Chicago Press, 1984.
- [19] M. A. Podurets, *Soviet Astron.* **8**, 19(1964); Ch. W. Misner and D. H. Sharp, *Phys. Rev.* **136B**, 571(1964); S. Hawking, *J. Math. Phys.* **9**, 958(1968); R. Geroch, *Ann. N Y. Acad. Sci.* **225**, 108(1973).
- [20] L. Szabados, *Living Rev. Relativity* **12**, 4 (2009).
- [21] S. Nishida and Y. Eriguchi, *Astrophys. J.* **427**, 429 (1994).
- [22] P. Jaranowski, P. Mach, E. Malec and M. Piróg, *Journal of Physics: Conference Series* **600**, 012011 (2015).
- [23] P. Mach, E. Malec and M. Piróg, *Acta Phys. Pol.* B43, 2141 (2012).
- [24] B. Gidas, W. M. Ni and L. Nirenberg, *Commun. Math. Phys.* **68**, 209(1979).
- [25] P. Chruściel, J. Jezierski and M. MacCallum, *Phys. Rev.* **D58**, 084001(1998).
- [26] J. Karkowski, E. Malec, K. Roszkowski and Z. Świerczyński, *Acta Phys. Pol.* **B40**, 273(2009).
- [27] E. Malec, *Acta Phys. Pol.* **B22**, 829 (1991).
- [28] E. Malec, *Phys. Rev. Lett.* **67** 949 (1991).
- [29] P. Koc and E. Malec, *Acta Phys. Pol.* **B23** 123 (1992).
- [30] P. Bizoń, E. Malec and N. Ó Murchadha, *Class. Quantum Grav.* **7** 1953 (1990).
- [31] P. Bizoń and E. Malec, *Phys. Rev. D* **40** 2559 (1989).
- [32] E. Malec and N. Xie, *Phys. Rev.* **D91**, 081501 (2015).
- [33] R. Schoen and S. T. Yau, *Commun. Math. Phys.* **90**, 575 (1983).
- [34] N. Ó Murchadha, *Phys. Rev. Lett.* **57**, 2466 (1986).
- [35] M. Khuri, *JHEP* **6**, 188 (2015).
- [36] I. Hachisu, *Astrophys. J. Suppl.* **61**, 479 (1986).
- [37] M. Hashimoto, Y. Eriguchi, K. Arai and E. Müller, *Astronomy and Astrophysics* **268**, 131 (2012).
- [38] R. Price, Ch. Markakis and J. L. Friedman, *J. Math. Phys.* **50**, 073505 (2009).